INTERNATIONAL JOURNAL FOR NUMERICAL METHODS IN FLUIDS
Int. J. Numer. Meth. Fluids **29**: 765–789 (1999)

TWO-DIMENSIONAL SIMULATIONS OF MAGMA ASCENT IN VOLCANIC CONDUITS

J.I. RAMOS*

Departamento de Lenguajes y Ciencias de la Computación, E.T.S. Ingenieros Industriales, Universidad de Málaga, Plaza El Ejido, s/n, 29013 Malaga, Spain

SUMMARY

A two-dimensional model for magma ascent in volcanic conduits is presented. The model accounts for the magma rheology, heat flux to the surrounding country rock, planar and axisymmetric geometries, and flow in the mushy region by means of a continuum mixture formulation that does not require keeping track of the liquid–solid interfaces. Numerical experiments for Newtonian and visco-plastic Bingham rheologies of magmas are presented as functions of the volumetric flow rate at the dyke's entrance and wall heat fluxes for both round conduits and fissures. It is shown that, depending on the magma rheology, dyke geometry, volumetric flow rate and wall heat flux, the magma may solidify along the original dyke's walls, thus reducing the available cross-sectional area to the flow, or the original dyke's walls may melt. It is also shown that the dyke's wall temperature may first increase and then decrease, and that the axial velocity profile exhibits a parabolic shape in the core region and a plug zone near the dyke's walls for Bingham rheologies. Copyright © 1999 John Wiley & Sons, Ltd.

KEY WORDS: magma; volcanoes; visco-plastic fluids; Bingham model; two-phase flows; solidification

1. INTRODUCTION

Magmas generated in the Earth's mantle rise to accumulate at the base of the colder brittle lithosphere. Sometimes the accumulated magma is tapped as the stress builds up and a new dyke is initiated. Owing to the buoyancy of the magma relative to that of the surrounding rock, the magma flows upwards and involves the interaction amongst buoyancy, viscosity, heat transfer, elastic deformation and fracture. For very long dykes, the dominant driving force is buoyancy, which leads to a viscosity–buoyancy balance, whereas the pressures required to produce elastic deformation of the walls are much less than the buoyancy forces; therefore, such dykes should be thought of as flexible conduits that dilate sufficiently to accommodate the magma flux arriving from below [1,2]. Furthermore, stresses are found to be significant only in the vicinity of the crack tip.

Volcanic eruptions display a rich variety of phenomena depending on the magma viscosity. Low viscosity magmas allow for degassing and flow, whereas more viscous magmas may result in explosive eruptions [3]. However, volcanic eruptions evolve in time in a complex manner, and the formation of fissures or dykes is the result of elastic and thermal processes in the surrounding rocks.

* Correspondence to: Departamento de Lenguajes y Ciencias de la Computación, E.T.S. Ingenieros Industriales, Universidad de Málaga, Plaza El Ejido, s/n, 29013 Malaga, Spain.

CCC 0271–2091/99/070765–25$17.50

Received December 1997
Revised March 1998

During volcanic eruptions, hot magma traverses a conduit from the magmatic source to the surface through cold crustal rocks. As a consequence, the magma may solidify. Similarly, in many industrial processes, such as injection moulding and continuous casting, hot fluid is forced to flow between cold boundaries against which solidification of the fluid can occur. In both cases, solidification of the fluid constricts the flow, which may become completely blocked. Since the rate of solidification depends on the convective heat transfer, and the fluid velocity in turn, depends on the cross-sectional area of the volcanic conduit, the fluid dynamics of magma during volcanic eruptions is strongly coupled to heat transfer and results in complex, non-linear, time-dependent phenomena.

Previous studies of volcanic eruptions include those based on heat conduction, and models that account for fluid motion. Spence and Turcotte [4] decoupled the fluid dynamics and heat transfer processes, and calculated the heat transfer and the solidification rates as if the magma were at rest; they, therefore, neglected any effect of advection, i.e. convective heat transfer. Their predictions indicate that the magma flow ceases in a matter of days. Bruce and Huppert [3] considered the flow of magma along a fissure at constant overpressure, and assumed laminar flow along an initially planar fissure of constant width, rigid walls and a single solidification temperature, below which the magma ceases to flow. They also specified the wall temperature, while the difference between the heat fluxes in the surrounding rocks and in the flowing magma was set equal to the product of the latent heat of solidification and the migration velocity of the liquid–solid interface. Their one-dimensional thermal model allows for the determination of the flow in the dyke and its evolution after the initial rock propagation and widening have taken place, and assumes that the flowing magma, its solid product and the country rock have identical thermal properties. Their two-dimensional fluid dynamics model is based on a Newtonian, laminar flow approximation, a parabolic axial velocity profile and a fixed pressure drop, and accounts for local solidification or melting.

Bruce and Huppert [3] showed that for basaltic magmas, the heat loss to the surrounding rocks leads to a fissure constricted by the magma solidifying at the walls and may end the eruption before the magma supply is exhausted. They also showed that, if the continual supply of heat by the magma exceeds the losses to the surrounding rocks, the initial solidification is reversed, and the walls of the fissure are progressively melted until the magma supply diminishes. Other studies include those of Lister [1,2] who investigated the solidification within a fluid-driven propagating crack embedded in an elastic solid, and employed a lubrication approximation in the heat and mass transfer equations. Lister [1,2] assumed that heat transfer in the solid is one-dimensional and interacts with the along-stream advection and cross-stream diffusion in the liquid. Lister and Dellar [5] considered the solidification of hot viscous fluids driven by a fixed pressure drop through initially planar or cylindrical channels embedded in cold rigid walls, and showed that at early times or far from the magmatic source, the flow starts to solidify and block the channel, whereas at later times, the supply of new hot fluid starts to melt back the initial chill layer. Their results indicate that, eventually, either solidification or meltback becomes dominant through the channel and the flow either ceases or continues until the magmatic source is exhausted depending on the thermal Peclet number, the Stefan number and a dimensionless solidification temperature.

Wylie and Lister [6] considered a pressure-driven viscous flow of an initially hot fluid through a planar channel with cold walls and a temperature-dependent viscosity, and showed that if the viscosity variations with temperature are sufficiently large, the relation-

ship between the pressure drop and the flow rate may be non-monotonic, and multiple steady states may exist. They also analyzed the linear stability of these flows and developed a cross-channel-averaged model to study the finite amplitude evolution of disturbances. Their results indicate that for high viscosities, some flows are unstable to three-dimensional (fingering) instabilities analogous to those of the Saffman–Taylor type. Helfrich [7] developed a model of magma flow in dykes and fissures based on averaged equations across the channel that does not account for the inertia terms in the linear momentum equations, but which predicts thermo-viscous fingering.

Other models for magma ascent include the two-dimensional one developed by Ramos and Dobran [8] who assumed that the magma ascends along a central conduit from the magma storage chamber, exsolving gases such as water vapor and carbon dioxide. Such a model includes a homogeneous, three-phase flow mixture, visco-elasto plastic effects due to the gas and vapor bubbles dissolved in the magma, and solidification and melting along the volcanic conduit, and predicts constriction and widening of the conduit for basaltic and andesitic magmas respectively, when the heat flux at the conduit's walls is specified. Therefore, the results of this model, which uses the same physical properties for both andesitic and basaltic magmas, are in qualitative agreement with those predicted by the one-dimensional model of Bruce and Huppert [3]. However, the model of Ramos and Dobran [8] assumes that there is constant flow of magma at the magmatic source and does not allow for complete blocking of the volcanic conduit; complete blocking may occur when the heat losses to the surrounding rocks are larger than the heat supplied by the flowing magma and the heat generated by viscous dissipation. Moreover, the nearly absence of non-vertical dykes within the first few kilometers of the surface of most volcanoes seem to imply that, at least in the superficial regions of volcanoes, three-dimensional effects are important. Furthermore, the crystal-bearing magma behaves as a non-Newtonian fluid with a yield stress, i.e. it behaves as a Bingham fluid when the crystal content is significant.

In this paper, a time-dependent, two-dimensional (planar or axisymmetric), two-phase continuum mixture [9] model for pressure-driven magma ascent in volcanic conduits is proposed. The model accounts for both the liquid and the solidified magma, and the mushy region near the solidification front, by using a continuum mixture formulation, and for the heat transfer between the magma and the surrounding rocks; it also accounts for Boussinesq effects associated with the dependence of the magma's density on the temperature and composition. Although, the model has been formulated to analyze several kinds of Newtonian and non-Newtonian fluid rheologies, the results presented here correspond to Newtonian and Bingham models of basaltic magmas. The model equations have been formulated so that they can be applied in the molten, single-phase liquid, the mushy region and the solidified magma. In order to accommodate the flow in the porous mushy region and the viscous flow in molten ones, the permeability–porosity relation proposed by Oldenburg and Spera [10] is employed. This relation makes the permeability small when the solid volumetric fraction is large, and infinity when it is small.

The two-dimensional model presented in this paper differs from previous ones [8] in that it accounts for non-Newtonian rheologies that depend on the temperature and void fraction, fully couples the heat transfer and fluid dynamics equations, uses a continuum mixture formulation, accounts for the porosity of the mushy region, and considers the heat transfer in the crustal rocks surrounding the volcanic fissure. However, it does not account for the elasticity of the crustal rocks surrounding the volcanic conduit.

2. GOVERNING EQUATIONS

The governing equations for the two-phase magma flow model employed here are based on a continuum mixture formulation [9] and a binary system with two components, and correspond to the conservation of mass, linear momentum, energy and mixture components, and may be written as

$$\frac{\partial \rho}{\partial t} + \nabla \cdot (\rho \boldsymbol{v}) = 0, \tag{1}$$

$$\frac{\partial}{\partial t}(\rho \boldsymbol{v}) + \nabla \cdot (\rho \boldsymbol{v}\boldsymbol{v}) = -\nabla p + \nabla \cdot \tau + \rho \mathbf{g} - \frac{\bar{\mu}_\mathrm{l}}{\bar{K}} \frac{\rho}{\rho_\mathrm{l}} (\boldsymbol{v} - \boldsymbol{v}_\mathrm{s}), \tag{2}$$

$$\frac{\partial}{\partial t}(\rho h) + \nabla \cdot (\rho \boldsymbol{v} h) = \nabla \cdot (k \nabla h) + \tau : \nabla \boldsymbol{v} - \nabla \cdot (\rho (h_\mathrm{L} - h)(\boldsymbol{v} - \boldsymbol{v}_\mathrm{s})), \tag{3}$$

$$\frac{\partial}{\partial t}(\rho f) + \nabla \cdot (\rho \boldsymbol{v} f) = \nabla \cdot (\rho_\mathrm{l} D_\mathrm{l} \alpha_\mathrm{l} \nabla f_\mathrm{l}) - \nabla \cdot (\rho (f_\mathrm{l} - f)(\boldsymbol{v} - \boldsymbol{v}_\mathrm{s})), \tag{4}$$

where t denotes time; p is the pressure; ρ, $\boldsymbol{v}$ and h denote the mixture density, velocity vector and enthalpy respectively; k is the mixture thermal conductivity; the subscripts l and s refer to liquid and solid phases respectively; α is a volumetric fraction in the two-phase mixture; D is the mass diffusivity; $\mathbf{g}$ is the gravitational acceleration; $\bar{K}$ is the permeability of the two-phase mushy region; ρf, ρf_l and ρf_s denote the solute concentration in the mixture, liquid phase and solid phase respectively, and therefore, f, f_l and f_s are the solute mass fractions in the mixture, liquid phase and solid phase, and $f_\mathrm{l} + f_\mathrm{s} = 1$; τ is the stress tensor; and, $\bar{\mu}_\mathrm{l}$ is related to the liquid's dynamic viscosity. The values of $\bar{K}$, and τ and $\bar{\mu}_\mathrm{l}$ will be specified later when dealing with the mushy region and the rheology of the magma.

The last term on the right-hand-side of Equation (2) accounts for the mushy region, which has been modelled as a porous medium according to Darcy's law. The mushy region was not considered in the two-dimensional formulation of Ramos and Dobran [8].

The Boussinesq approximation, i.e.

$$\rho \mathbf{g} = \rho_\mathrm{l} \mathbf{g}(1 + \beta_\mathrm{T}(T - T_\mathrm{ref}) + \beta_\mathrm{s}(f - f_\mathrm{ref})), \tag{5}$$

was used in the momentum equation, where β_T and β_s denote the coefficients of thermal and solutal expansion respectively, and the subscript ref denotes reference values.

The mixture density may be expressed as

$$\rho = \alpha_\mathrm{s} \rho_\mathrm{s} + \alpha_\mathrm{l} \rho_\mathrm{l}, \tag{6}$$

whereas, if ϕ stands for $\boldsymbol{v}$, f and h,

$$\phi = X_\mathrm{s} \phi_\mathrm{s} + X_\mathrm{l} \phi_\mathrm{l}, \tag{7}$$

where

$$\alpha_\mathrm{s} + \alpha_\mathrm{l} = 1, \qquad X_\mathrm{s} + X_\mathrm{l} = 1, \tag{8}$$

$$f = f_\mathrm{s} X_\mathrm{s} + f_\mathrm{l} X_\mathrm{l}, \tag{9}$$

$$X_i = \frac{\rho_i \alpha_i}{\rho}, \quad i = \mathrm{s}, \mathrm{l}, \tag{10}$$

$$k = \alpha_\mathrm{s} k_\mathrm{s} + \alpha_\mathrm{l} k_\mathrm{l}, \tag{11}$$

$$\bar{K} = G\frac{K_0\alpha_l^3}{(1-\alpha_l)^2}. \tag{12}$$

X denotes mass fraction, K_0 is a constant for the Blake–Kozeny–Carmen equation for permeability, which corresponds to $G=1$ and $\boldsymbol{v}_s = \mathbf{0}$.

Both $\bar{K}$ and $\bar{\mu}_l$ have been introduced to account for the porosity of the mushy region. Away from this region in the liquid, $G=0$ and $\bar{\mu}_l$ is identical to the liquid viscosity μ_l. Here, the expressions proposed by Oldenburg and Spera [10] have been used, i.e.

$$\bar{\mu}_l = \mu_l\frac{1}{(1-2F\alpha_s)^2}, \tag{13}$$

$$F = 0.5 - P, \qquad G = (0.5+P)^{-4}, \tag{14}$$

$$P = \frac{1}{\pi}\arctan(100(\alpha_s - \alpha_{sc})), \tag{15}$$

where $\alpha_{sc} = 0.5$ is the critical volumetric fraction of solid material at which the balance of forces in the mushy region changes from being controlled by buoyancy and viscosity to the one controlled by buoyancy and permeability. Note that, for $\alpha_s < \alpha_{sc}$, $\bar{K}$ is a large value, the mushy region is nearly a liquid and the last term on the right-hand-side of the momentum equation is small, i.e. the porosity effect of the mushy region is small. On the other hand, if $\alpha_s > \alpha_{sc}$, the last term on the right-hand-side of the momentum equation is important and Darcy's effects are accounted for in the mushy region. Note also that, for two-phase systems in which there is no relative motion between the melt and the solid, the Darcy terms in the momentum equations are zero.

The enthalpies of the liquid and solid phases are related to the temperature through the following equations

$$h_l = \int_0^T C_{pl}\,\mathrm{d}T + L, \tag{16}$$

$$h_s = \int_0^T C_{ps}\,\mathrm{d}T, \tag{17}$$

where L is the latent heat of phase change and C_p denotes the specific heat at constant pressure. Furthermore, it may be easily shown that

$$\bar{C}_p = \bar{C}_{ps}X_s + \bar{C}_{pl}X_l, \tag{18}$$

$$h = \bar{C}_p T + X_l L, \tag{19}$$

where $\bar{C}_p$ denotes an average specific heat, e.g.

$$\bar{C}_{ps} = \frac{1}{T}\int_0^T C_{ps}(T)\,\mathrm{d}T. \tag{20}$$

In the above equations, it has been assumed that the melt and solid may coexist at the same location and have the same temperature. This assumption may be incorrect because phase changes of multicomponent mixtures occur over a temperature range and, in addition to heat transfer, mass transfer may result in solute redistribution, microsegregation and macrosegregation; these phenomena are not considered here. However, the coexistence of melt and solid allows the treatment of the two-phase flow magma mixture as a whole; therefore, there is no need to track melt–solid interfaces. Moreover, the continuum mixture theory employed here assumes local thermodynamic equilibrium so that the solid and liquid concentrations may be

determined from the phase diagram, i.e. given the mixture mass fraction f and the temperature T at any point and time, both the mass fractions and the concentrations of the liquid and solid can be determined as functions of these two variables, which are governed by Equations (3) and (4) and are non-linearly coupled through Equations (6)–(17); they are also non-linearly coupled with Equations (1) and (2). This non-linear coupling demands high numerical and computational efforts if realistic phase diagrams are employed in the numerical simulations. Although realistic phase diagrams may be handled by the numerical method employed here, the simplified phase diagram, shown in Figure 1, is considered, which represents a linearization of that for a binary system with two components but does not account for the solids formed when molecules of one component are incorporated into the lattice of the other component; these solids appear between the left skirt of the realistic phase diagram and the left vertical axis, and between the right skirt of the realistic phase diagram and the right vertical axis. The linearization of the realistic phase diagram results in a linear relation between T and f, rather than the non-linear ones that occur when realistic phase diagrams are used.

For the simplified phase diagram of Figure 1, it is easily shown that

$$X_l = 1 - \frac{1}{1-k_p}\frac{T-T_{liq}}{T-T_m}, \tag{21}$$

$$f_l = \frac{f}{k_p + X_l(1-k_p)}, \qquad f_s = k_p f_l, \tag{22}$$

$$T_{liq} = T_m + (T_e - T_m)\frac{f}{f_e}, \tag{23}$$

where T_{liq} denotes the liquidus temperature, k_p is the equilibrium partition ratio, and the subscripts e and m refer to the eutectic point and melt respectively.

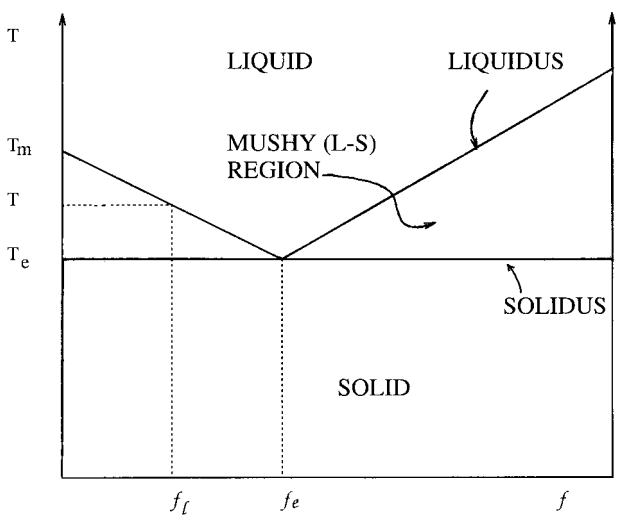

Figure 1. Idealized phase diagram for binary materials.

3. NUMERICAL METHOD

The equations presented in the previous section were applied to study the magma ascent in planar and axisymmetric configurations. These equations were discretized in a staggered grid by means of a conservative control volume formulation that uses central differences for the diffusion-like terms and upwind or central differences for the advective ones depending on the magnitude of the cell or mesh Reynolds numbers. This formulation results in a system of non-linear, ordinary differential equations for the mass, linear momentum, energy and mixture components in each computational cell, which were transformed into non-linear algebraic ones by discretizing the time derivatives by means of the backward (implicit) Euler method. Due to the implicit character of the discretization and the non-linear coupling between the dependent variables, an underrelaxation technique and a line-by-line procedure were used to solve the difference equations for each dependent variable by sweeping the computational domain axially starting at the conduit's inlet, as many times as necessary until convergence was achieved. Once the flow field was found to converge, the time was advanced. Although only results for steady flows are presented here, the numerical method may be used to analyze transient phenomena, such as those associated with time-dependent boundary conditions at the conduit's entrance; moreover, the use of a time-dependent strategy to solve a steady state problem increases the diagonal dominance of the discretized equations and facilitates their numerical solution.

The pressure was determined by combining the continuity and momentum equations, and solving a Poisson equation for the pressure [11]. This equation accounted for the convective and diffusive terms, body forces and Darcy's terms that appear in the momentum equation. Moreover, for the low Reynolds numbers associated with the magma flows considered in this paper, it was found that, except in very large computational cells, central differences were used for the convection terms.

The scalar-dependent variables were defined at the grid points, while the velocity components were evaluated at midpoints in order to calculate the convective fluxes accurately. Some numerical difficulties were initially experienced due to the non-linear coupling between the mixture composition and temperature through the equilibrium phase diagram and Equations (3) and (4). These difficulties were solved by first determining the temperature and concentration fields from the solution of Equations (3), (4) and (19) using the guessed values of the liquid mass fraction. These values were then used to determine the liquid mass fraction in an inner loop by using the iterated values of the mixture temperature and concentration as follows. Instead of determining the liquid mass fraction from the temperature, the temperature was written as a function of the liquid mass fraction (cf. Equation (21)), i.e.

$$T = \frac{T_{\mathrm{liq}} - T_{\mathrm{m}}(1-k_{\mathrm{p}})(1-X_{\mathrm{l}})}{1-(1-k_{\mathrm{p}})(1-X_{\mathrm{l}})}, \tag{24}$$

and the resulting equation was substituted into Equation (19), which was solved iteratively by means of a quasi-linearization technique to determine X_{l} until convergence was achieved. The resulting liquid mass fraction was again used in Equations (3) and (4), and this procedure was repeated until convergence of all the flow variables was reached in every computational cell or volume. Furthermore, at the eutectic point, phase change was assumed to occur isothermally, i.e. the temperature at any point can decrease below the eutectic point only if the material at that point has completely solidified [12].

Heat conduction in the rocks surrounding the dyke was analyzed by means of two different models. The first model solves a two-dimensional heat conduction equation in the rocks

subject to specified temperature conditions sufficiently far away from the dyke, i.e. a temperature at infinity, and a heat transfer coefficient, and both the temperature and heat flux normal to the interface between the solid rocks and the domain that includes the volcanic conduit are continuous at that interface. In the second model, Equations (1)–(4) were applied to determine the heat transfer in the surrounding rocks, where the velocity is zero and only the energy equation is relevant, by treating the surrounding rocks as a fluid of very large dynamic viscosity. In this second model, the temperature in the solid rocks was determined by specifying their temperature field sufficiently far away from the dyke, i.e. a temperature at infinity, and a heat transfer coefficient, and both the temperature and heat flux normal to the interface between the solid rocks and the domain that includes the volcanic conduit are continuous at that interface. This second approach allows one to consider the liquid and solidified magma and the surrounding rocks with the same formulation as a whole, and is of special relevance when the continuous supply of heat by the flowing magma exceeds the losses into the surrounding rocks, and the walls of the dyke melt until the magma supply diminishes.

Both models were used to determine the heat flux from/to the surrounding rocks and the Biot number based on the temperature of the surrounding rocks far away from the dyke, by assuming that the flowing magma and the surrounding rocks have the same thermal properties; this assumption, however, is an approximation since the country rocks surrounding a volcanic conduit vary with depth. The results of these models were in qualitative accord with each other, and the heat fluxes determined from them were used with the two-dimensional fluid dynamics equations presented here to determine the magma motion and solidification when partial blocking of the dyke occurs; therefore, in this paper, the heat fluxes determined from models that account for heat conduction in the solid rocks that surround a volcanic conduit were employed to determine the magma ascent and solidification. This approach has the advantage that only the flow in the original conduit must be resolved, and results in substantial computational savings. A similar approach was followed for the case that the dyke's walls melt; however, in this case, the heat flux conditions were not imposed at the original dyke's walls, but at a radial location where there is no melting of these walls.

The specification of either numerically determined or experimental heat fluxes at the dyke's walls is more physically plausible than the specification of the temperature at the walls, i.e. Dirichlet's boundary conditions, especially when there is magma solidification, because these fluxes take into account the heat exchanges between the flowing magma and the surrounding rocks. Moreover, an isothermal (constant temperature) boundary condition at the original dyke's walls is not adequate when the magma solidifies because it would not account appropriately for the heat conduction in the solidified magma at the dyke's walls. In any event, the formulation presented here is able to deal with Dirichlet, Neumann and Robin's boundary conditions at the original dyke's walls.

Numerical experiments were also performed with specified heat flux conditions at the dyke's walls, such as those proposed by Carrigan *et al.* [13]. In all the cases considered, however, it was assumed that, initially, the dyke's geometry was either a fissure or a round conduit. The evolution of the flow and solidified magma was followed in time until a stationary state was reached. Such a stationary state can be easily identified when the heat supplied by the hot magma is larger than the heat losses to the country rocks for specified entrance conditions. However, when blocking occurs, the entrance conditions depend on time in such a manner that the magma flow stops when the dyke is blocked. In order to illustrate both (partial) blocking and melting of the volcanic conduit, the length of the dyke was specified so that no complete blocking occurs for the constant entrance conditions considered here, and the boundary conditions at the dyke's exit were determined by assuming fully developed laminar flow there

and accounting for the difference between the inlet flow rate and the solidification rate. The exit boundary conditions for the temperature and mixture's mass fraction were determined by imposing that the gradients of these variables along the streamlines were zero at the exit. These conditions are approximations to the true ones because when the magma solidifies along the dyke's walls, the available cross-sectional area for the flow decreases and the surface area for the flow and heat transfer diminishes.

In order to accurately resolve the flow field, the grid points were concentrated at the inlet and near the original dyke's walls; however, due to the large aspect ratio of a volcanic conduit, the number of grid points in the axial direction must be very large, otherwise the cells may have large aspect ratios, which may lead to either numerical instabilities or inaccurate results. Although the qualitative physical trends of the magma ascent may be predicted by using a grid of about 100 along and 30 grid points across the volcanic conduit respectively, more accurate results may be obtained by decreasing the grid spacing in the direction along the conduit. Such calculations were performed by employing a domain decomposition technique that decomposes the computational domain into several overlapping subdomains in the axial and transverse directions and carried out in a distributed computing environment.

Calculations were performed with several grids in order to obtain grid-independent results. The number of grid points and their locations depended on the conduit's entrance conditions, heat flux at the dyke's walls and fluid rheology. For the volcanic conduits considered here, which have an aspect ratio of 200, the coarsest grid employed in the calculations consisted of 64×1200 unevenly spaced grid points for half a conduit.

Convergence was reached when the global residuals of the integrated mass, linear momentum and energy equations were equal to or less than 10^{-4} times the fluxes of these quantities at the conduit's entrance, and when the flow variables at a monitoring point did not change by more than 10^{-6} in 250 successive iterations.

4. PRESENTATION OF RESULTS

The two-phase flow model presented in this paper has been applied to determine the ascent of Newtonian [13] and Bingham or visco-plastic models [14] of magmas in axisymmetric and planar fissures for different volumetric flow rates $\dot{V}$, and wall heat fluxes, $\dot{q}_w$, and some sample results are presented in this section. Unless otherwise stated, $f(0, x, r) = 0.36$, $T_m = 1665$ K, $T_e = 1547$ K, $k_p = 0.1$, $\rho_s = \rho_l = 2500$ kg m^{-3}, $C_{pl} = 1000$ J kg^{-1} K^{-1}, $L = 300000$ J kg^{-1}, $f_e = 0.8$, $p(0, x, r) = p_0 = 10^5$ bar, $T(0, x, r) = T_0 = 1610$ K, $K_0 = 5.10^{-11}$ m^2, $\mu_s = 10^{30}$ kg m^{-1} s^{-1}, $D_l = 10^{-8}$ m^2 s^{-1}, $k_l/\rho_l C_{pl} = 7 \times 10^{-7}$ m^2 s^{-1}, and $\beta_s = \beta_T = 0$. Only results for volcanic conduits 200 m long, 1 m wide fissures, and round conduits of 1 m in diameter are presented here, since as stated in the previous section, the length of the dyke was specified so that no full blocking occurs for the conditions considered in the paper. If full blocking occurred, the downstream boundary conditions employed here would not be valid, a front-tracking technique would have to be used to determine and follow the magma front, and the boundary conditions at the conduit's entrance would be functions of time. Note that fissures are channels.

Since the volumetric flow rate at the dyke's inlet was specified and the length of the volcanic conduit was selected so that no full blocking of the volcanic conduit occurred, the calculations were performed in such a manner that there is outflow and the normal derivatives of the dependent variables at the outflow boundary were set to zero. Calculations were also performed with time-dependent volumetric flow rates at the inlet, although they are not reported here.

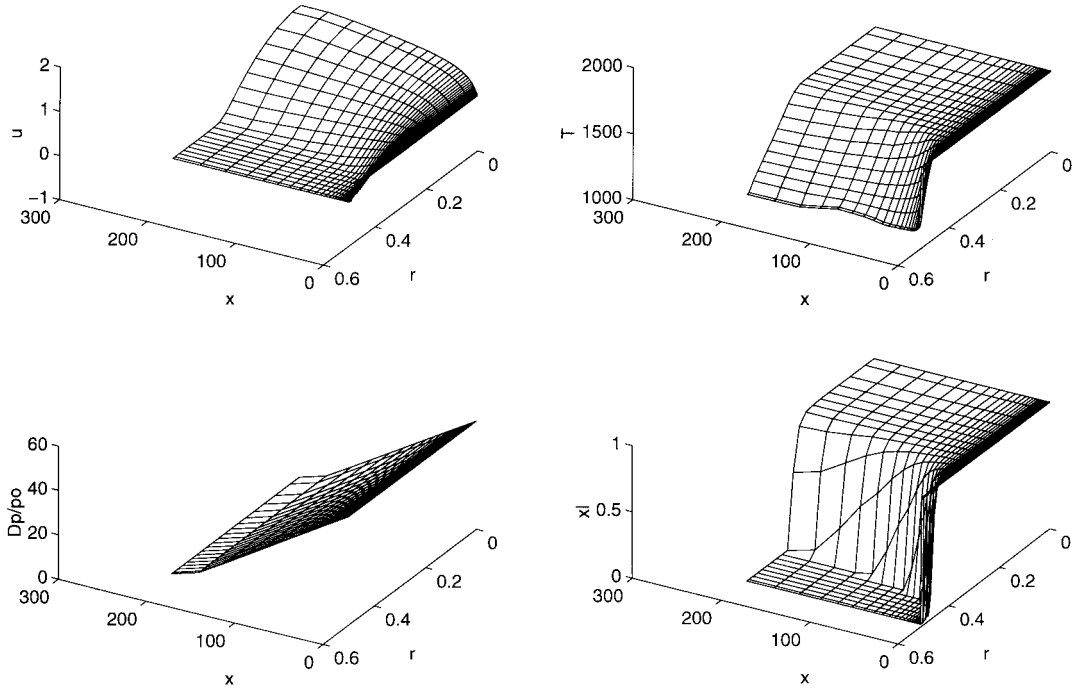

Figure 2. Axial velocity component (top left), temperature (top right), pressure difference referred to entrance pressure (bottom left) and liquid mass fraction (bottom right) in a round conduit as functions of the transverse coordinate at selected locations along the dyke for the Newtonian model of basaltic magmas. ($\dot{V} = 0.2\ \mathrm{m^3\ s^{-1}}$, $\dot{q}_w = 500\ \mathrm{J\ m^{-2}\ s^{-1}}$).

The axial velocity profile at the dyke's inlet was assumed to be flat because the magma emerges from a chamber that is much larger than volcanic conduits and, therefore, the axial velocity profile is not parabolic at the conduit's entrance.

It must be pointed out that, since the flow of magma in both planar fissures and round conduits was considered, the transverse co-ordinate measured from the conduit's centerline is referred to as either r or y in the following figures.

It should be noted that if the heat supplied by the flowing magma is higher than the heat losses to the volcanic conduit's walls, the latter may melt. As a consequence, the available cross-sectional area for the flow would increase and both the magma's axial velocity and the viscous dissipation would decrease. Thereafter, the rate and duration of the volcanic eruption would be controlled by the decay in the driving pressure difference as well as by the possible closure of the dyke because of the resulting subsidence of the volcanic edifice. On the other hand, if the heat supply by the flowing magma is smaller than the heat losses to the conduit's walls, the magma will solidify along the walls, thus decreasing the available cross-sectional area and, for a constant pressure drop along the volcanic conduit, the magma velocity and the viscous dissipation would increase. This increase in viscous dissipation may cause high temperatures locally, which may cause melting of the chill layer.

For the sake of brevity, the units used throughout are those of the MKS system, and the temperature is measured in Kelvin.

4.1. Newtonian models of basaltic magmas

For basaltic magmas, the liquid viscosity in MKS units is [13]

$$\mu_l = 10^{-6} \exp\left(\frac{26\,170}{T}\right), \tag{25}$$

and these magmas were assumed to be Newtonian, i.e.

$$\tau = 2\mu_l \boldsymbol{D}, \quad \boldsymbol{D} = \frac{1}{2}(\nabla \boldsymbol{v} + (\nabla \boldsymbol{v})^T), \tag{26}$$

where $\boldsymbol{D}$ is the strain or deformation rate tensor, and the superscript T denotes transpose. Some sample results for these magmas are presented in Figure 2 for round conduits, a (constant) heat flux at the conduit wall, $\dot{q}_w$, of 500 and $\dot{V} = 0.2$, at selected axial locations along the conduit. It should be noted that in order to illustrate in a clear manner the more important features of magma flows, only results in a small fraction of the grid points employed in the calculations are shown in the following figures.

Figure 2 indicates that the flat axial velocity profile at the dyke's entrance becomes a parabolic one in the core region a short distance downstream, whose maximum value increases along the conduit, which becomes constricted on account of the magma solidification at the dyke's walls.

Figure 2 also shows that the magma temperature is identical to that of the entrance in the core flow, and drops almost linearly to the dyke's temperature, which varies along the dyke.

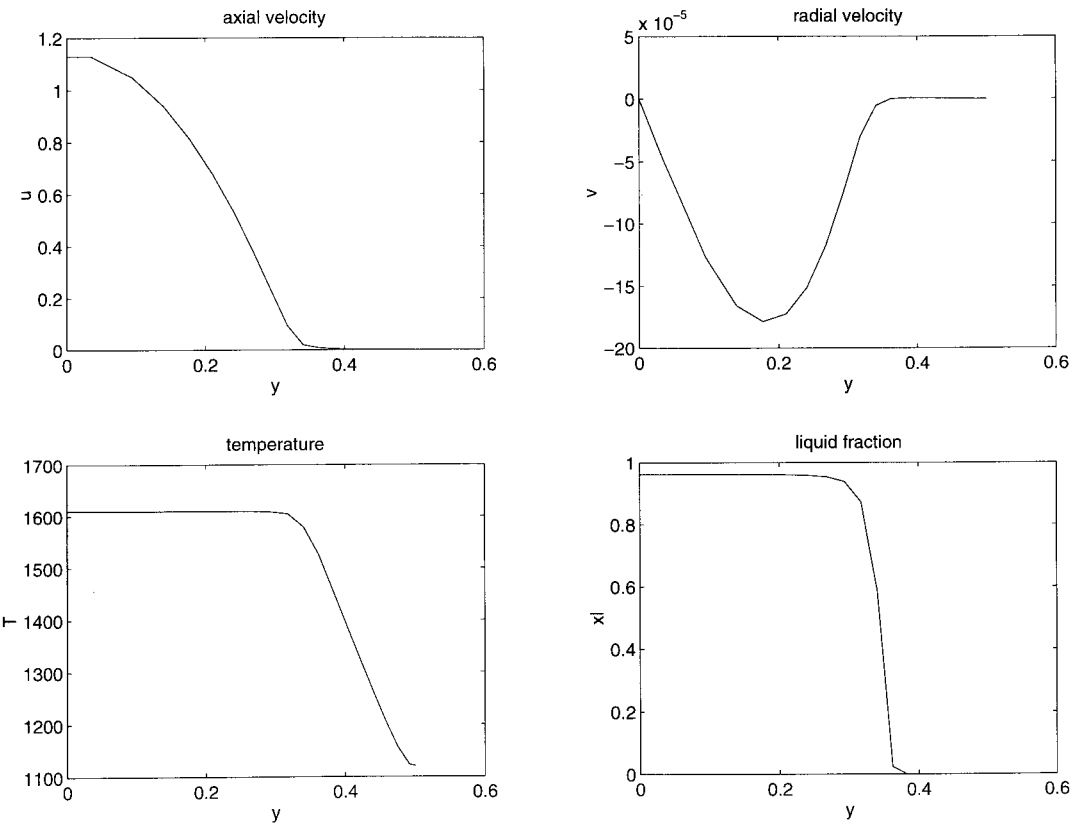

Figure 3. Axial velocity component (top left), radial velocity component (top right), temperature (bottom left) and liquid mass fraction (bottom right) in a round conduit as functions of the transverse coordinate at selected locations along the dyke for the Newtonian model of basaltic magmas ($\dot{V} = 0.2$ m^3 s^{-1}, $\dot{q}_w = 500$ J m^{-2} s^{-1}).

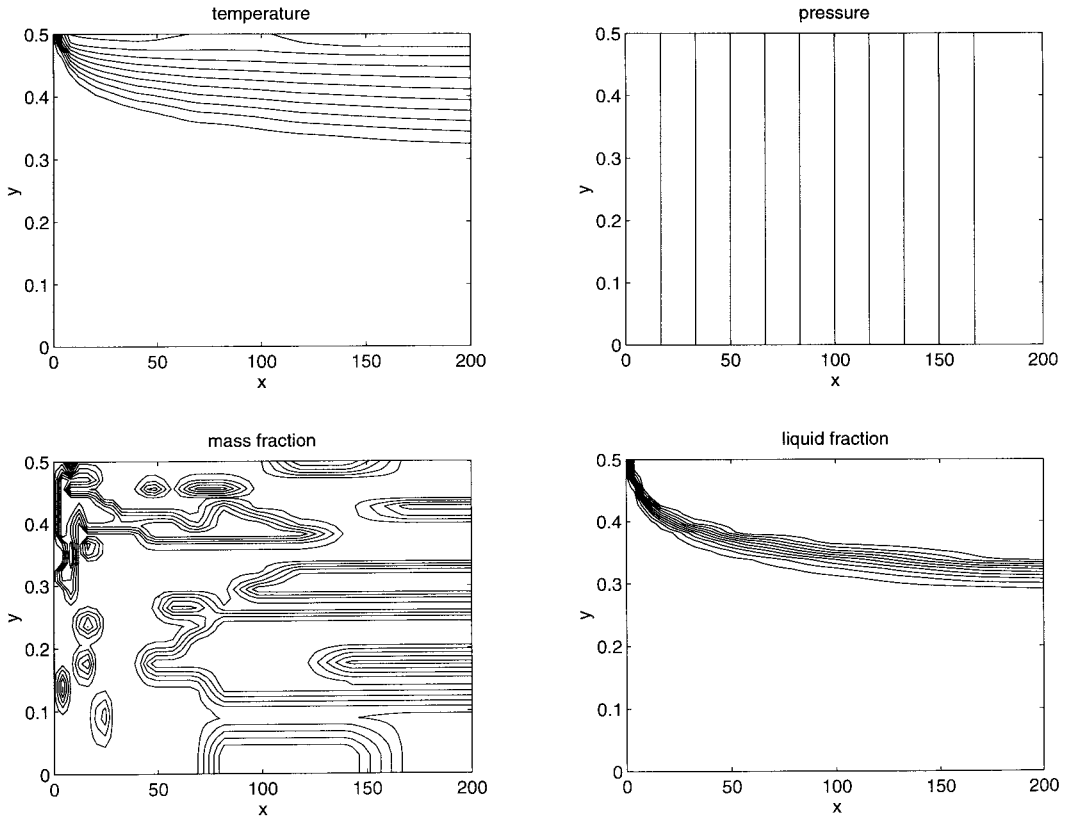

Figure 4. Isotherms (top left), isobars (top right), isocontours of mixture mass fraction (bottom left) and isocontours of liquid mass fraction (bottom right) in a round conduit as functions of the transverse and axial co-ordinates for the Newtonian model of basaltic magmas. ($\dot{V} = 0.2\ \mathrm{m^3\,s^{-1}}$, $\dot{q}_w = 500\ \mathrm{J\,m^{-2}\,s^{-1}}$).

The liquid mass fraction illustrated in Figure 2 also indicates the solidification of the magma along the conduit's walls and the constriction of the cross-sectional area, while the ratio of the difference between the entrance pressure and the local one to the entrance pressure almost varies linearly in accordance with a linear or hydrostatic pressure distribution, except near the entrance due to the transition of the velocity profile from a flat to a parabolic profile. These trends are more clearly illustrated in Figure 3, which corresponds to $x = 100$ m, and indicates that the radial velocity component is very small.

Figure 3 indicates that, at $x = 100$ m, the axial velocity profile is almost parabolic in the flowing magma and zero in the solidified layer close to the conduit's wall, and that the flowing magma has an available cross-sectional area that corresponds to a circle whose radius is about 0.34 m. This implies that, if the amount of solidified magma is neglected, the maximum axial velocity at this axial location corresponding to mass conservation is about $1.10\ \mathrm{m\,s^{-1}}$, i.e. it is about four times larger than the inlet velocity. This result is consistent with that of Figure 3 and illustrates the axial flow acceleration due to the flow constriction owing to the magma solidification. Moreover, mass conservation was satisfied at each conduit's cross-section.

The isocontours of some flow variables are illustrated in Figure 4, which indicates that the magma solidification occurs from the dyke's entrance, the pressure distribution is uniform at each cross-section along the volcanic conduit, and a rapid solidification occurs near the entrance as indicated in the liquid mass fraction isocontours.

Similar trends to those shown in Figures 2–4 have also been observed for smaller volumetric flow rates at the dyke's entrance and higher heat fluxes at the dyke's walls except that the thickness of the solidified layer increases as the volumetric flow rate is decreased and/or the heat flux to the walls is increased.

For $\dot{V} = 0.3$ and $\dot{q}_w = 500$, and $\dot{V} = 0.2$ and $\dot{q}_w = 200$, the dyke's wall temperature is higher than for $\dot{V} = 0.2$ and $\dot{q}_w = 500$ due to the fact that the heat losses to the surrounding rocks are smaller than the heat supplied by the flowing magma and the heat generated by viscous dissipation as shown in Figure 5, which clearly indicates that the wall temperature increases downstream from the entrance; this temperature increase may cause melting of the surrounding rocks. Figure 5 also shows that the liquid mass fraction is equal to one along the conduit's original wall, i.e. there is no magma solidification along the conduit's walls, and that the axial velocity profile undergoes a rapid transition from a flat shape at the conduit's entrance to a parabolic one downstream. However, a higher heat flux at the conduit's wall results in solidified magma; for example, for $\dot{V} = 0.3$, solidified magma at the dyke's wall was observed for $\dot{q}_w \geq 1500$.

Figure 6 shows the cross-sectional profiles of some of the variables illustrated in Figure 5 at $x = 100$ m, and indicates that the axial velocity profile is a parabola at $x = 100$ m, the radial velocity component is very small, and the temperature profile shows a relative maximum near the wall. The isocontours presented in Figure 7 illustrate that the pressure is uniform at each cross-section along the volcanic conduit, and that temperature of the conduit's wall increases immediately from the entrance.

Similar trends to those shown in Figures 2–7 have also been observed for fissures, except that melting of the dyke's wall was observed for $\dot{V} = 0.2$ and $\dot{q}_w = 500$. Magma solidification

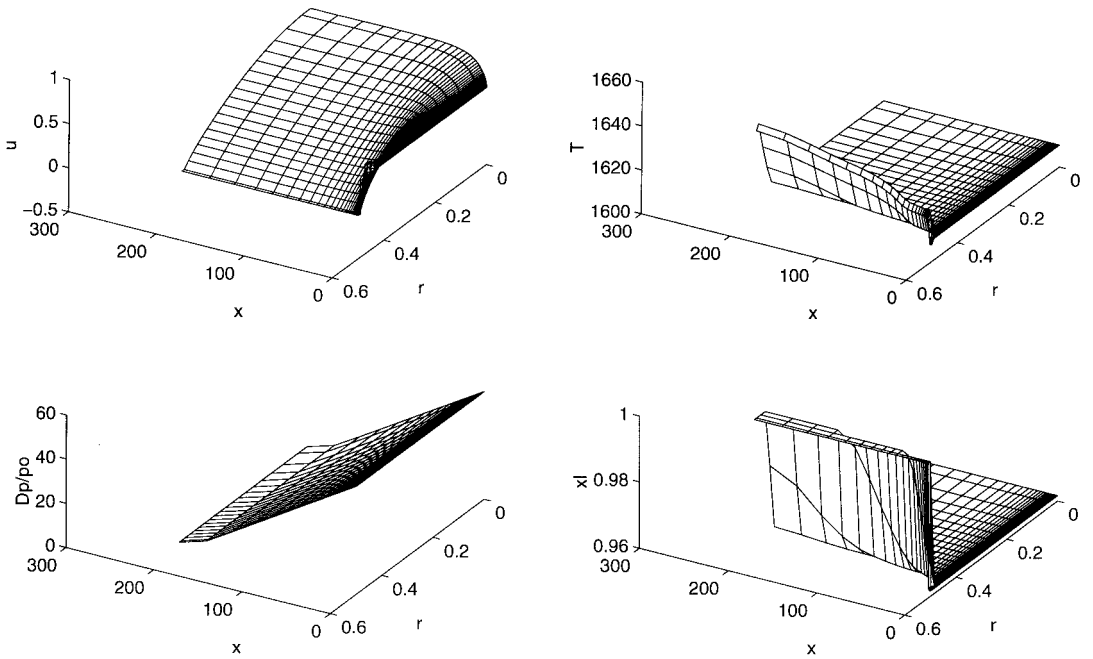

Figure 5. Axial velocity component (top left), temperature (top right), pressure difference referred to entrance pressure (bottom left) and liquid mass fraction (bottom right) in a round conduit as functions of the transverse co-ordinate at selected locations along the dyke for the Newtonian model of basaltic magmas ($\dot{V} = 0.2$ m^3 s^{-1}, $\dot{q}_w = 200$ J m^{-2} s^{-1}).

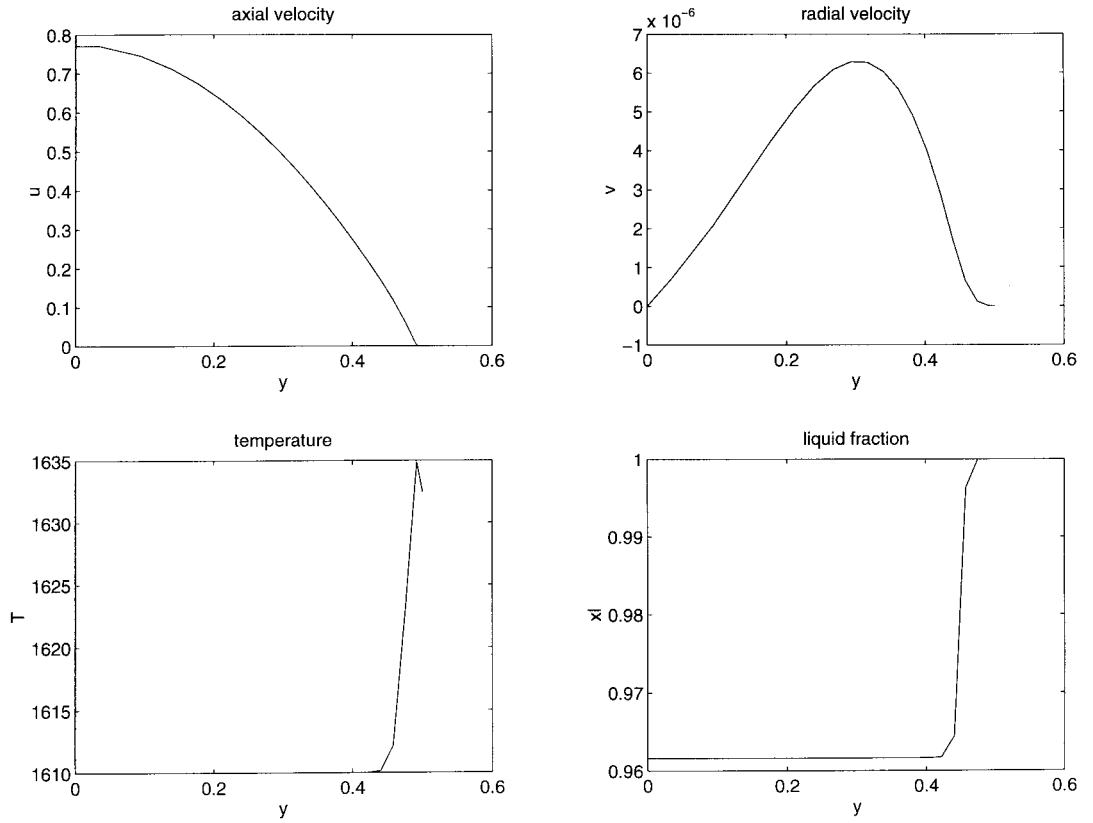

Figure 6. Axial velocity component (top left), radial velocity component (top right), temperature (bottom left) and liquid mass fraction (bottom right) in a round conduit as functions of the transverse co-ordinate at $x = 100$ m for the Newtonian model of basaltic magmas ($\dot{V} = 0.2$ m^3 s^{-1}, $\dot{q}_w = 200$ J m^{-2} s^{-1}).

was found to occur for the same flow rate and higher heat fluxes, and for the same heat flux and lower volumetric flow rates. The temperature of the dyke's wall was also observed to increase for fissures as the volumetric flow rate was increased and/or the heat flux to the conduit's walls was decreased.

A summary of the conduit's wall temperature is presented in Figure 8 for both round conduits and fissures, several wall heat fluxes and entrance volumetric flow rates. This figure clearly illustrates that the magma solidifies along the conduit except for $(\dot{V}, \dot{q}_w) = (0.3, 500)$ for round conduits, and (0.2, 500) and (0.3, 500) for fissures. Figure 8 also shows that melting back of the dyke followed by magma solidification occurs for $(\dot{V}, \dot{q}_w) = (0.3, 1500)$ for fissures. The results presented in Figure 8 and others not shown here indicate the wall temperature is a function of both the heat flux, i.e. the temperature of the surrounding rocks far away from the dyke or the Biot number, and the volumetric flow rate. In addition, the distance required for the solidification of the magma to be noticeable decreases as the wall heat flux is increased and as the volumetric flow rate is decreased.

The results presented here are in qualitative agreement with the predictions of the simplified model proposed by Bruce and Huppert [3] for basaltic magmas.

4.2. *Bingham models of basaltic magmas*

For magmas that exhibit a Bingham rheology, the model proposed by Pinkerton and Stevenson [l4] was employed. This model was developed for magmas at subliquidus temperatures and may be written as

$$\tau = 2\left(\mu_{\mathrm{m}} + \frac{\tau_{\mathrm{y}}}{|\dot{\gamma}|}\right)\boldsymbol{D}, \quad |\dot{\gamma}| > |\dot{\gamma}_{\mathrm{c}}|, \tag{27}$$

$$\tau = 2\mu_{\mathrm{r}}\boldsymbol{D}, \quad |\dot{\gamma}| \leq |\dot{\gamma}_{\mathrm{c}}|, \tag{28}$$

where

$$|\dot{\gamma}| = \left(\frac{1}{2}\,\boldsymbol{D} : \boldsymbol{D}\right)^{1/2}, \tag{29}$$

$$\mu_{\mathrm{m}} = \mu_{\infty} + \frac{\mu_0 - \mu_{\infty}}{1 + |\dot{\gamma}|(\mu_0 - \mu_{\infty})/B}, \tag{30}$$

$$\mu_0 = \mu_{\mathrm{L}}\left(\frac{\alpha_{\mathrm{s,max}}}{\alpha_{\mathrm{s,max}} - \alpha_{\mathrm{s}}}\right)^{2.5}, \tag{31}$$

$$\mu_{\infty} = \mu_{\mathrm{L}} \exp\left(\left(2.5 + \left(\frac{\alpha_{\mathrm{s}}}{\alpha_{\mathrm{s,max}} - \alpha_{\mathrm{s}}}\right)^{0.48}\right)\frac{\alpha_{\mathrm{s}}}{\alpha_{\mathrm{s,max}}}\right), \tag{32}$$

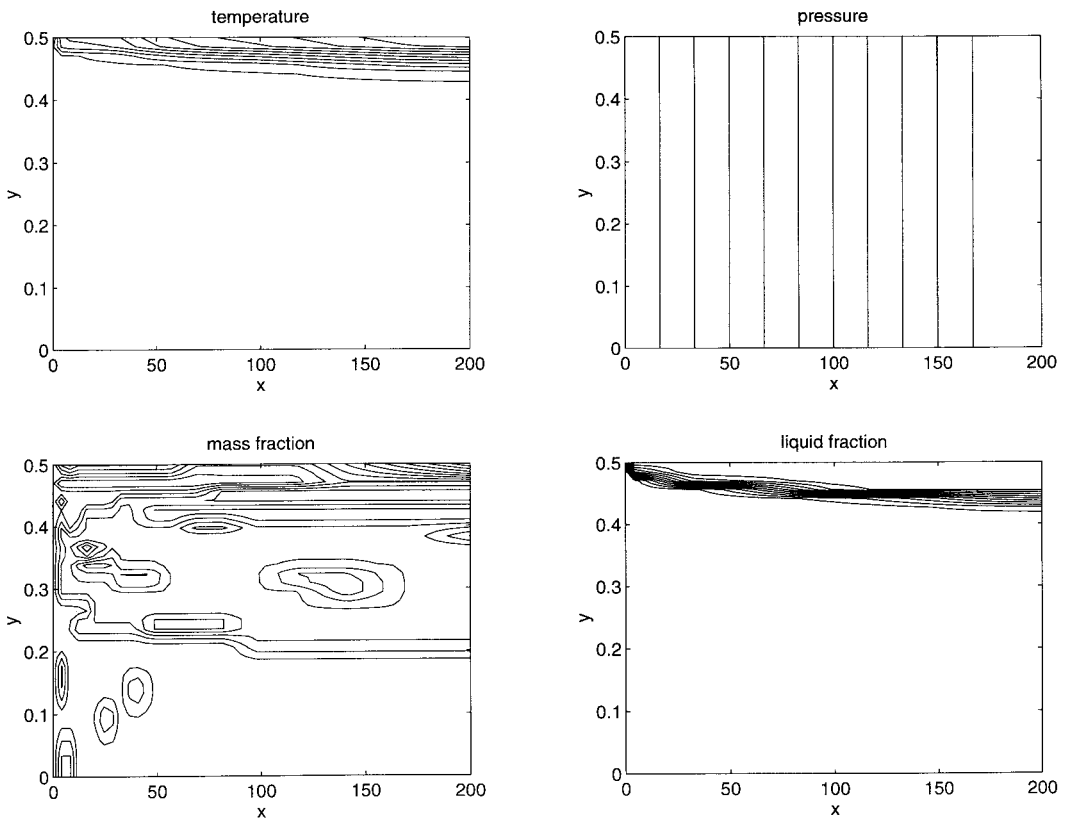

Figure 7. Isotherms (top left), isobars (top right), isocontours of mixture mass fraction (bottom left) and isocontours of liquid mass fraction (bottom right) in a round conduit as functions of the transverse and axial co-ordinates for the Newtonian model of basaltic magmas ($\dot{V} = 0.2\ \mathrm{m^3\,s^{-1}}$, $\dot{q}_{\mathrm{w}} = 200\ \mathrm{J\,m^{-2}\,s^{-1}}$).

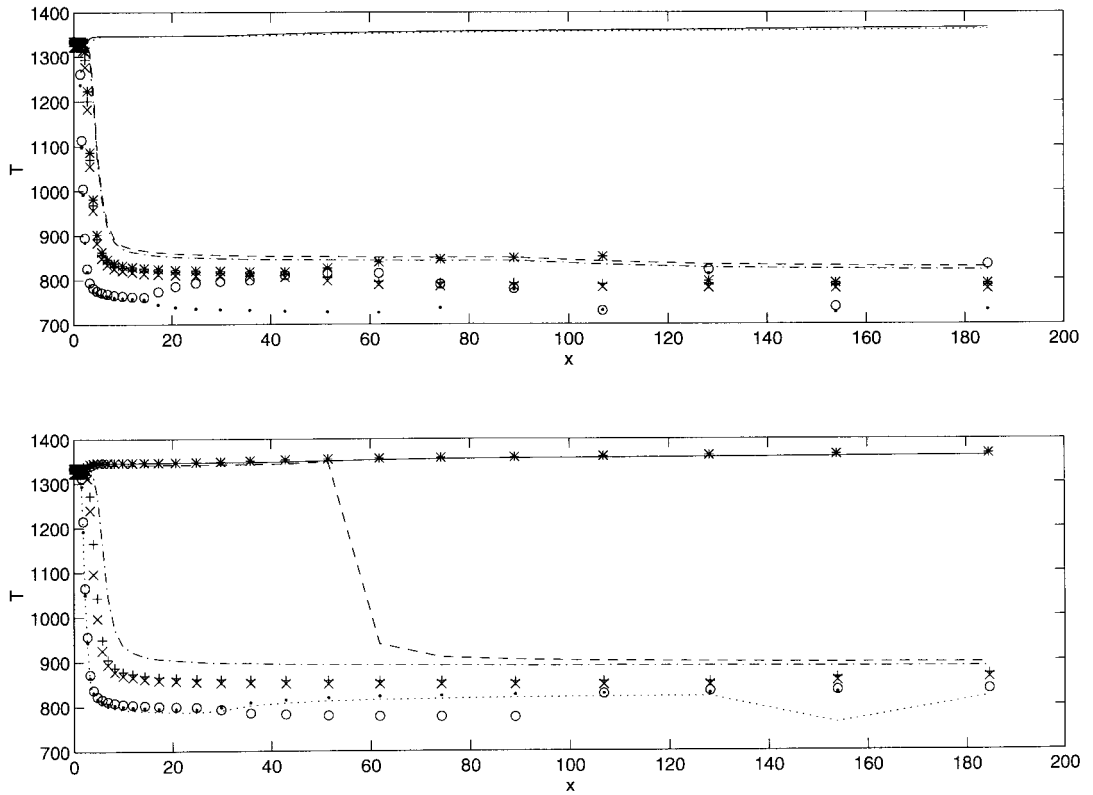

Figure 8. Wall temperature (°C) for round conduits (top) and fissures (bottom) along the dyke for the Newtonian model of magmas for an inlet temperature of 1337°C; $(\dot{V}, \dot{q}_w) = (0.2, 500)$, $*$; (0.2, 1500), $+$; (0.2, 3000), $\times$; (0.1, 500), $\circ$; (0.1, 1500), $\bullet$; (0.1, 3000), dotted line; (0.3, 500), solid line; (0.3, 1500), dashed line; (0.3, 3000), dashed-dotted line).

$$\tau_y = 1.26\rho_l g\left(\frac{d_p}{\alpha_{s,max} - \alpha_s}\right)\left(\frac{\alpha_{s,max}}{1 - \alpha_{s,max}}\right)^2 \frac{1}{\sigma^2 \xi^{1.5}}, \tag{33}$$

$$B = 0.066\tau_y\left(\frac{\alpha_{s,max}^2}{\alpha_{s,max} - \alpha_s}\right)\left(\frac{\mu_L^2}{\rho_l \tau_y d_p^2}\right)^{0.21}, \tag{34}$$

$$\alpha_{s,max} = 0.634, \qquad \xi = 0.34, \qquad \sigma = 1.88, \qquad \mu_L = 50, \tag{35}$$

the subscripts y, c and max denote yield, critical and maximum respectively, and the reference viscosity μ_r is at least $1000\mu_m$.

$\dot{\gamma}_c$ can be calculated by equating the stresses from Equations (27) and (28) and solving the resulting quadratic equation, which depends on α_s, which in turn, depends on the solution of Equations (1)–(4).

The value of d_p in Equations (34) and (35) is related to the solid volumetric fraction as follows. If N is the number of particles per unit volume and these are assumed to be spherical, then

$$d_p = \left(\frac{6\alpha_s}{\pi N}\right)^{1/3}. \tag{36}$$

Therefore, this model accounts for visco-plastic effects since it exhibits Newtonian and plastic or Bingham characteristics through μ_m and the yield stress respectively. However, the Bingham

model of basaltic magmas employed here differs from those usually employed in the literature [15], e.g.

$$\hat{\tau} = \eta\dot{\gamma}, \quad \hat{\tau} \geq \tau_0, \tag{37}$$

$$\dot{\gamma} = 0, \quad \hat{\tau} < \tau_0, \tag{38}$$

where

$$\dot{\gamma} = \left(\frac{1}{2}\boldsymbol{D} : \boldsymbol{D}\right)^{1/2}, \qquad \hat{\tau} = \left(\frac{1}{2}\tau : \tau\right)^{1/2}, \tag{39}$$

$$\eta = \mu_0 + \frac{\hat{\tau}}{\dot{\gamma}}, \tag{40}$$

since there is always a Newtonian contribution to the stress tensor through μ_m and μ_r in Equations (27) and (28) respectively. As a consequence, the model employed here, which is based on experimental data, does not suffer from the limitations of the standard one at the centerline where the shear strain rate is zero and there is a problem with the shear stress. It must be pointed out, however, that the limitations of the standard model at the centerline can be avoided by introducing a limiting value for the strain rate in an analogous manner to Equation (28).

As indicated above, the rheology of visco-plastic magmas in Pinkerton and Stevenson's model [14] depends on two factors N and μ_r. For $\mu_r = 10^8$, no results could be obtained for heat fluxes ranging from 50 to 3000, and N ranging from 10^7 to 10^{11} for both round conduits and fissures. For $\mu_r = 10^6$, results could be obtained for a wall heat flux of 50 and N ranging from 10^7 to 10^9 for both fissures and round conduits. In these cases, however, the wall temperature was observed to reach a value higher than 2600 K at $x = 100$ m, the pressure was not uniform at each cross-section, the axial velocity profile was characterized by a parabola in the core region and a plug flow profile with a non-zero value near the wall, and the wall temperature was found to be nearly equal to that at the entrance for $x \leq 60$ m and then it increased downstream. Moreover, the axial velocity profile underwent large variations along the conduit's axis. Furthermore, for $\mu_r = 10^6$ and $N \geq 10^{10}$, the wall temperature was found to reach the unrealistic value of more than 4000 K. These results indicate that for the same value of μ_r, the higher the value of N the higher the wall temperature.

Parametric studies were also performed for $\mu_r = 10^4$, $10^4 \leq N \leq 10^6$, $50 \leq \dot{q}_w \leq 3000$, $0.1 \leq \dot{V} \leq 0.2$, and round and planar volcanic conduits. The results of these studies, which are not shown here, indicate that the wall temperature at $x = 200$ m was at most 10° higher than the entrance's temperature, the temperature and the liquid mass fraction profiles were almost uniform except for a small gradient near the conduit's wall, and the axial velocity profile was almost flat with a steep gradient near the walls. Similar trends to the ones just described were also found for $\mu_r = 10^5$ and 10^7, $10^4 \leq N \leq 10^6$, $50 \leq \dot{q}_w \leq 3000$, $0.1 \leq \dot{V} \leq 0.2$, and round volcanic conduits and fissures. Moreover, the parametric studies performed for different volumetric flow rates and wall heat fluxes including those experimentally determined by Carrigan *et al.* [13] for round conduits and fissures indicate that Pinkerton and Stevenson's Bingham rheology is extremely sensitive to N or d_p. This is not surprising because the characteristics of their rheological model were determined by melting magmas collected in volcanic sites and performing the corresponding rheological measurements on them, and the rheological characteristics of the remelted magmas may be different from those of the original ones.

For $\mu_r = 10^5$, $(\dot{V}, \dot{q}_w) = (0.1, 500)$ and round conduits, the axial velocity profile underwent a rapid transition from its flat shape to a parabolic one, followed by a further transition to a parabolic profile in the core and a plug flow near the wall. The velocity of the plug flow and the dyke's wall temperature increased downstream, the liquid mass fraction at the wall was one, the distance required for the second flow transition was not a monotone function of N, and the wall temperature decreased as N decreased from 10^9 to 10^7. The highest temperature was observed near the wall for $N = 10^9$ and was about 1800 K. Furthermore, for $N = 10^7$, the second flow transition to a parabolic flat profile occurred at about $x = 100$ m, whereas for $N = 10^9$ and 10^8, it occurred at $x = 40$ and 20 m respectively. Similar trends were also observed for the same values of N in fissures, except that the wall temperature was higher in the latter.

Figure 9 shows some sample results for $\mu_r = 10^5$, $N = 10^8$, $(\dot{V}, \dot{q}_w) = (0.1, 500)$ and round conduits, clearly exhibits the two flow transitions described above, and illustrates that the wall temperature increases along the dyke. As indicated previously, the wall temperature increases as N is increased. The cross-sectional profiles of Figure 9 at $x = 100$ m are presented in Figure 10, which shows that the magma temperature increases near the wall, the small value of the radial velocity component, and the plug flow near the wall, while Figure 11 shows that it takes a distance of about 25 m for the wall's temperature to rise. Similar trends to those shown in Figures 9–11 have been observed in fissures, except that the wall temperature is higher in the latter.

Based on the above results and further numerical experiments not reported here, calculations were performed for $\mu_r = 10^4$ and 10^5 and N ranging from 10^7 to 10^9 as function of the volumetric flow rate and the heat flux. Some sample results are presented in Figures 12–14, which correspond to $(\dot{V}, \dot{q}_w) = (0.2, 100)$, and $N = 10^9$, 10^8 and 10^7 respectively. These figures

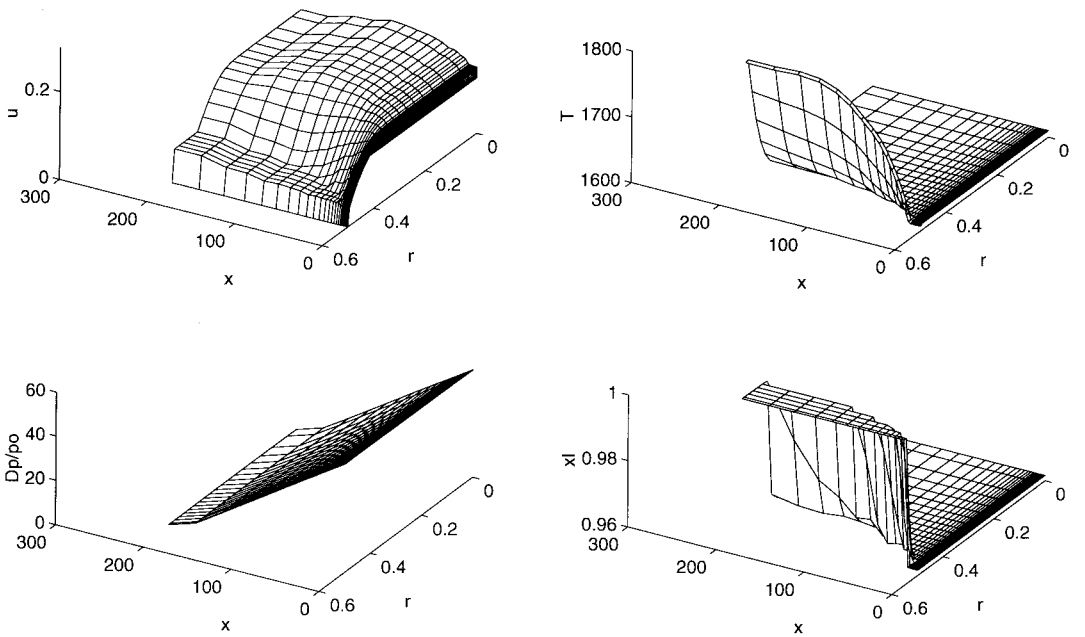

Figure 9. Axial velocity component (top left), temperature (top right), pressure difference referred to entrance pressure (bottom left) and liquid mass fraction (bottom right) in a round conduit as functions of the transverse co-ordinate at selected locations along the dyke for the Bingham's model of basaltic magmas ($\dot{V} = 0.1$ m^3 s^{-1}, $\dot{q}_w = 500$ J m^{-2} s^{-1}, $\mu_r = 10^5$ kg m^{-1} s^{-1}, $N = 10^8$).

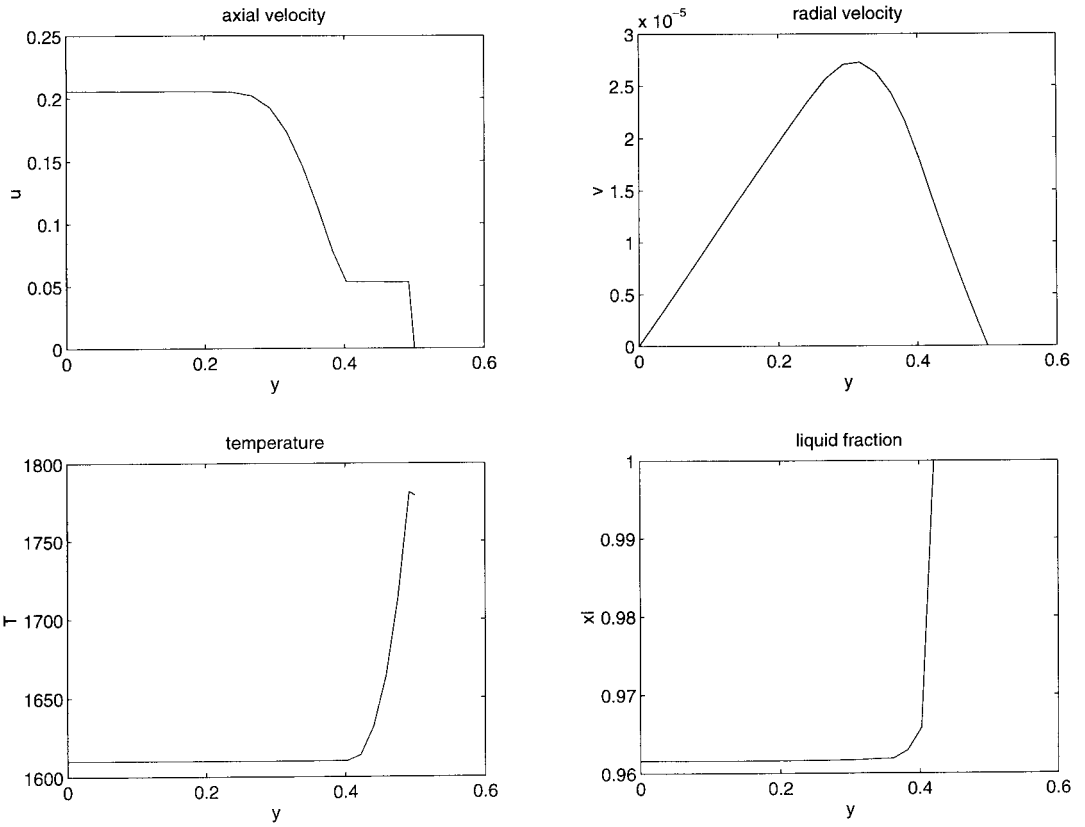

Figure 10. Axial velocity component (top left), radial velocity component (top right), temperature (bottom left) and liquid mass fraction (bottom right) in a round conduit as functions of the transverse coordinate at $x = 100$ m for the Bingham's model of basaltic magmas ($\dot{V} = 0.1\ \mathrm{m^3\,s^{-1}}$, $\dot{q}_w = 500\ \mathrm{J\,m^{-2}\,s^{-1}}$, $\mu_r = 10^5\ \mathrm{kg\,m^{-1}\,s^{-1}}$, $N = 10^8$).

clearly illustrate that the temperature of the conduit's wall increases as N is increased, and the transition of the flow from a flat profile to a parabolic one and then to a parabolic one in the core flow and a plug flow near the dyke. The increase in the temperature of the original conduit's walls may cause melting of the surrounding rocks and, therefore, an increase in the cross-sectional area with the consequent decrease in axial velocity and viscous dissipation until either the magma supply decreases or the volcanic edifice collapses owing to its subsidence.

Figures 12–14 also indicate that the axial velocity of the plug flow increases downstream and that, initially, the wall temperature slightly drops below its inlet value. The distance required for melting of the dyke's walls to occur increases as N is decreased. Similar trends to those exhibited in Figures 12–14 have also been observed for fissures except that the wall temperature is higher in the latter.

Figures 15 and 16 show the wall temperature as a function of the volumetric flow rate, heat flux and N for round conduits and fissures respectively, and indicates that the wall temperature of fissures is higher than that of round conduits, and the wall temperature decreases as N is decreased and the heat flux is increased. Figures 15 and 16 also indicate that the wall temperature starts rising after a distance from the entrance which increases as N is decreased, and that the trends of the wall temperature are the same for round conduits and fissures.

The results presented in this section for both Newtonian and Bingham rheologies indicate that when the heat supplied by the flowing magma is smaller than the heat losses to the

surrounding rocks, there is solidification of magma along the conduit's walls for Newtonian rheologies. However, even for $(\dot{V}, \dot{q}_w, N) = (0.1, 3000, 10^7)$ and round conduits, no magma was found to solidify for the visco-plastic Bingham model employed here, whereas for the same volumetric flow rate and heat flux, the Newtonian model predicted magma solidification. This difference between the Newtonian and Bingham models of basaltic magmas is associated with Equations (27) and (28) which, as stated above, include Newtonian and/or visco-plastic contributions, and indicates that the experimentally determined rheology of the Bingham model [14] employed here may not be accurate to predict the ascent of magmas in volcanic conduits because one should expect magma solidification for small volumetric heat fluxes and/or large heat fluxes at the conduit's walls.

Both the numerical results presented here and the simulations of andesitic magmas performed by Ramos and Dobran [8] strongly suggest that simpler models of pressure driven magma ascent in volcanic conduits may be developed since the radial velocity component is small, volcanic conduits are longer than their diameters, the Reynolds number is small, and axial diffusion is smaller than the radial one. These simpler models may be obtained by employing a long-wave, lubrication or slender approximation similar to that of Wylie and Lister [6], a viscous scaling for the pressure, and perturbation techniques with the slenderness ratio as the perturbation parameter. To leading order in the perturbation parameter, it can be

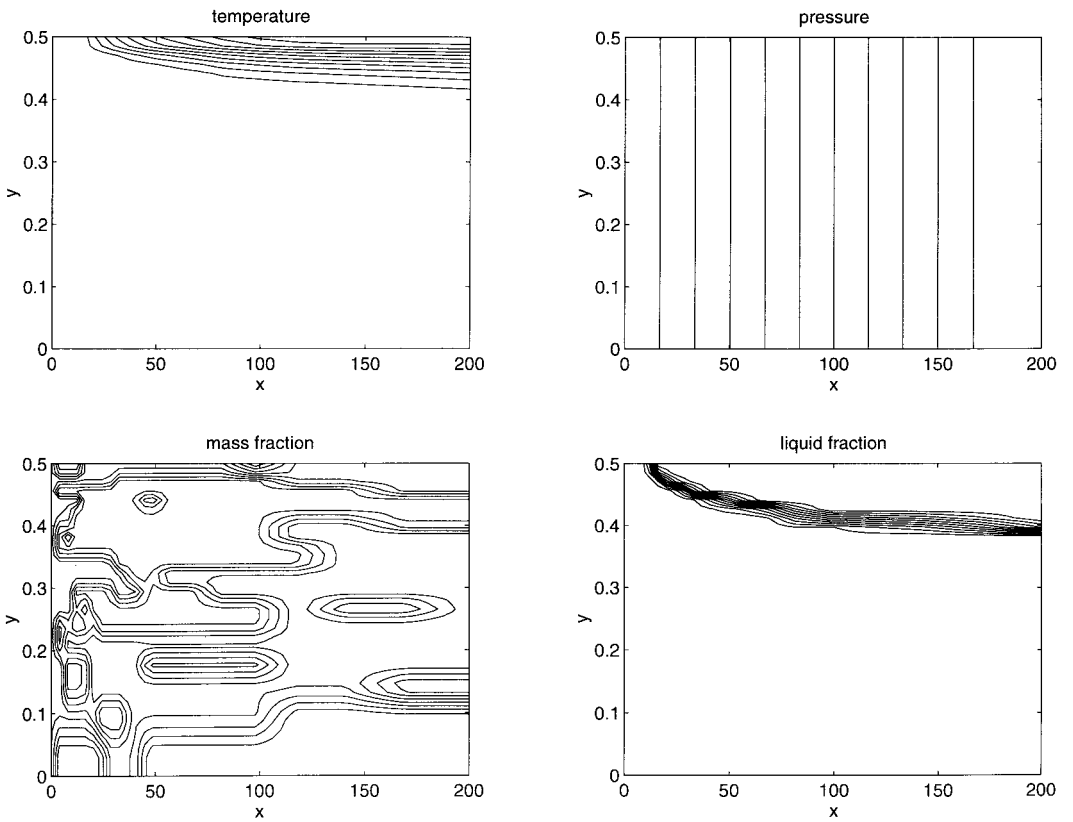

Figure 11. Isotherms (top left), isobars (top right), isocontours of mixture mass fraction (bottom left) and isocontours of liquid mass fraction (bottom right) in a round conduit as functions of the transverse and axial co-ordinates for the Bingham's model of magmas ($\dot{V} = 0.1\ \mathrm{m^3\,s^{-1}}$, $\dot{q}_w = 500\ \mathrm{J\,m^{-2}\,s^{-1}}$, $\mu_r = 10^5\ \mathrm{kg\,m^{-1}\,s^{-1}}$, $N = 10^8$).

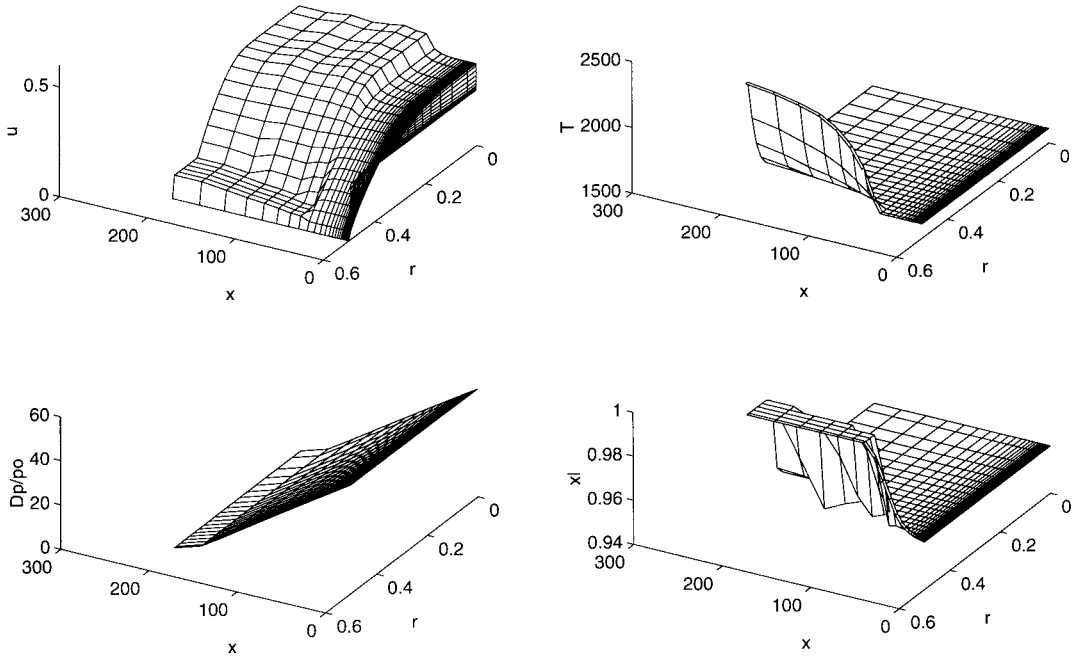

Figure 12. Axial velocity component (top left), temperature (top right), pressure difference referred to entrance pressure (bottom left) and liquid mass fraction (bottom right) in a round conduit as functions of the transverse co-ordinate at selected locations along the dyke for the Bingham's model of basaltic magmas ($\dot{V} = 0.2$ m^3 s^{-1}, $\dot{q}_w = 500$ J m^{-2} s^{-1}, $\mu_r = 10^5$ kg m^{-1} s^{-1}, $N = 10^9$).

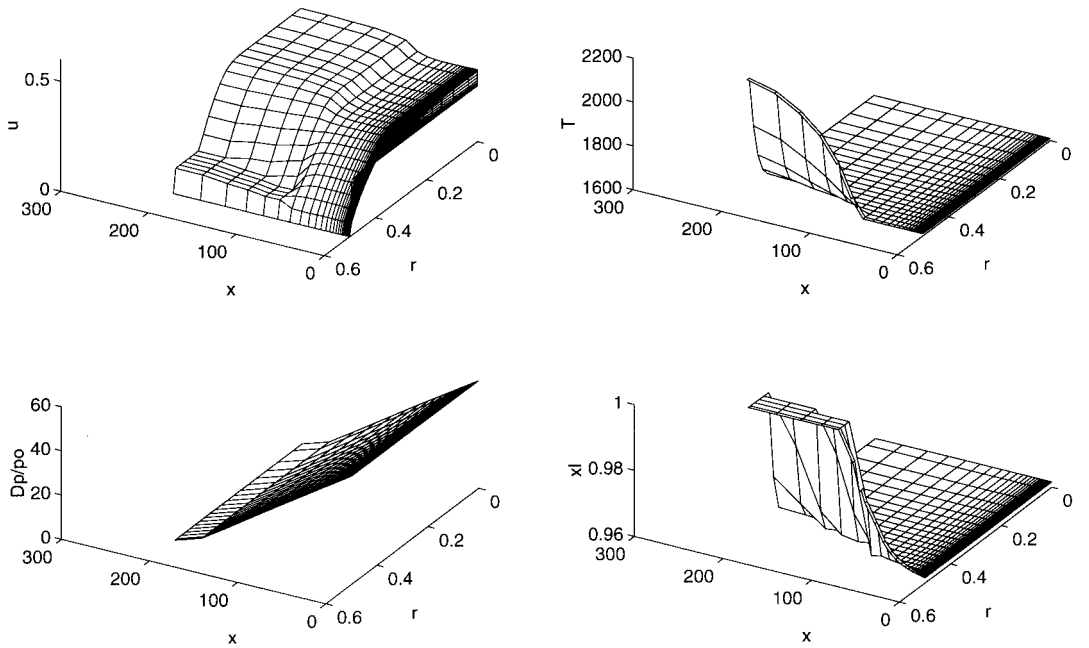

Figure 13. Axial velocity component (top left), temperature (top right), pressure difference referred to entrance pressure (bottom left) and liquid mass fraction (bottom right) in a round conduit as functions of the transverse co-ordinate at selected locations along the dyke for the Bingham's model of basaltic magmas ($\dot{V} = 0.2$ m^3 s^{-1}, $\dot{q}_w = 500$ J m^{-2} s^{-1}, $\mu_r = 10^5$ kg m^{-1} s^{-1}, $N = 10^8$).

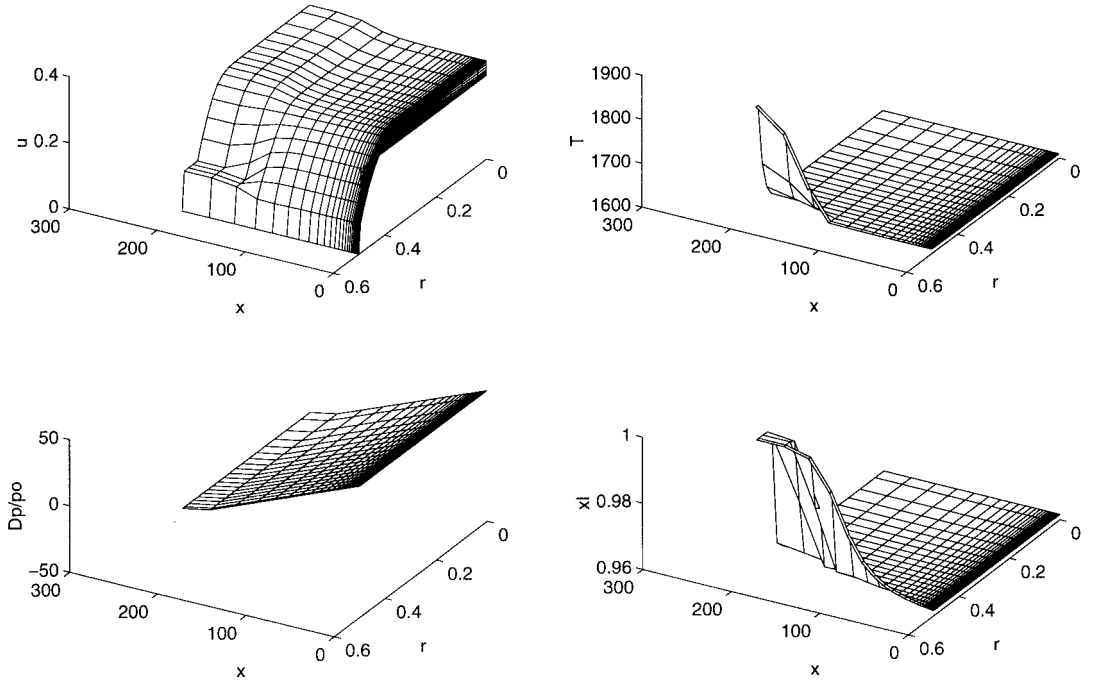

Figure 14. Axial velocity component (top left), temperature (top right), pressure difference referred to entrance pressure (bottom left) and liquid mass fraction (bottom right) in a round conduit as functions of the transverse co-ordinate at selected locations along the dyke for the Bingham's model of basaltic magmas ($\dot{V} = 0.2$ m^3 s^{-1}, $\dot{q}_w = 100$ J m^{-2} s^{-1}, $\mu_r = 10^5$ kg m^{-1} s^{-1}, $N = 10^7$).

easily seen that the pressure is a linear function of the co-ordinate along the volcanic conduit and the axial velocity component is only a function of the radial co-ordinate, although it depends in a strong non-linear fashion on the temperature through the magma's dynamic viscosity.

5. CONCLUSIONS

The effects of the magma rheology, volumetric flow rate, heat flux and dyke geometry on magma ascent in volcanic conduits have been investigated numerically by means of a two-dimensional, continuum mixture formulation, which accounts for Boussinesq effects, porous flow in mushy regions and magma solidification, but which does not require keeping track of melt–solid interfaces. It has been shown that for a constant volumetric flow rate at the dyke's entrance, the magma may either solidify along the dyke and constrict the flow or melt the surrounding rocks, thus widening the original dyke's cross-sectional area depending on the heat fluxes to the surrounding rocks and the heat supplied by the flowing magma. In both cases, it has been found that either blocking or melting of volcanic conduits depends on the volumetric flow rate, heat flux, dyke geometry and magma rheology.

For Newtonian models of magmas and the volumetric and heat fluxes considered in this paper, melting of the surrounding rocks was observed for the experimentally determined (estimated) heat fluxes at the volcanic conduit's walls. Magma solidification along the dyke for Newtonian models of magmas, however, was found to occur at high heat fluxes.

A visco-plastic Bingham model of magmas, which includes the effects of the solid particles through the solid void fraction on the yield stresses, has also been used. This model was found to depend critically on the number of solid particles per unit volume and a reference viscosity. Larger reference viscosities were found to yield no convergence of the numerical algorithm, whereas for lower ones, it was found that the wall temperature decreases as the number of solid particles per unit volume decreases. This Bingham model also shows that the axial velocity profile undergoes a first transition from a flat shape to a parabolic one, and then a second transition to a parabolic profile in the core flow and a plug flow near the dyke. The velocity of the plug flow was found to increase along the dyke. However, it was found that the experimentally determined rheology employed here may not be adequate for predicting the ascent of magmas in volcanic conduits because it is unable to predict magma solidification even for small volumetric flow rates and/or large heat fluxes to the surrounding rocks.

In addition to melting of the surrounding rocks and magma solidification along the dyke, it was found that the magma may first rise, increasing the surrounding rocks' temperature and then solidify depending on the volumetric flow rate, magma rheology, dyke geometry and heat flux. Therefore, in order to accurately predict the ascent of magmas in volcanic conduits, it is

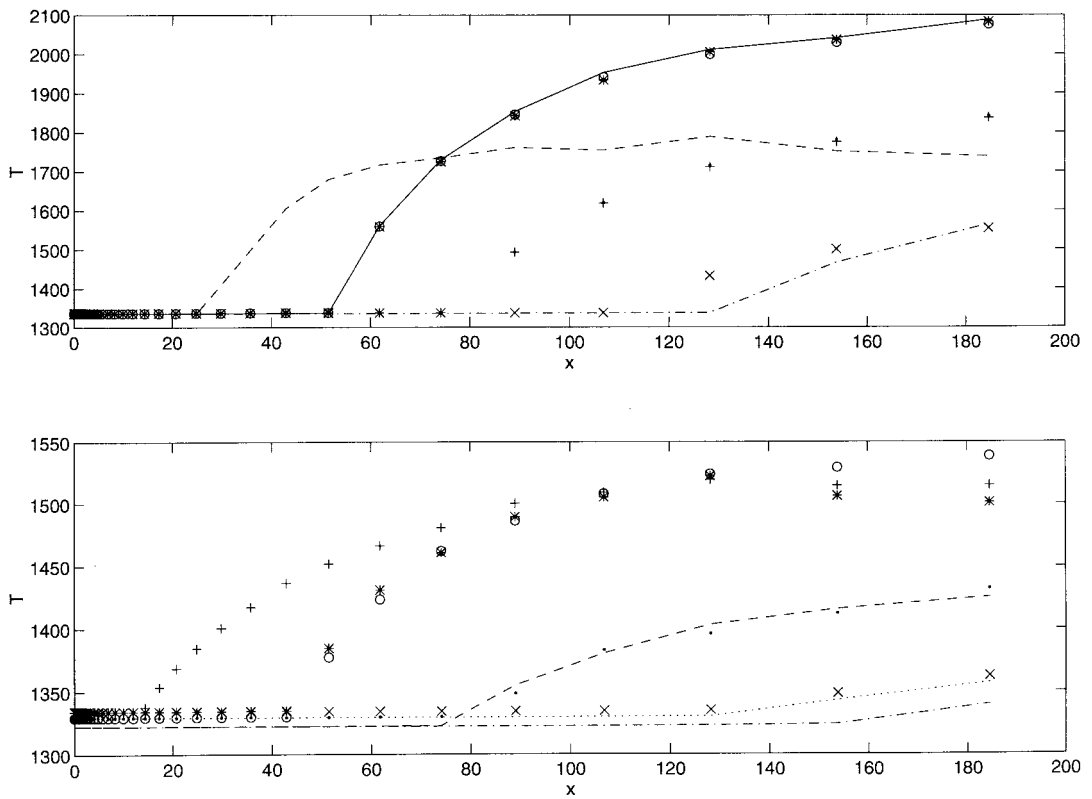

Figure 15. Wall temperature (°C) for round conduits along the dyke for the Bingham's model of magmas for an inlet temperature of 1337°C; (Top: $(\dot{V}, \dot{q}_w, N) = (0.2, 50, 10^9)$, $*$; $(0.2, 50, 10^8)$, $+$; $(0.2, 50, 10^7)$, $\times$; $(0.2, 100, 10^9)$, $\circ$; $(0.2, 50, 10^8)$, $\bullet$; $(0.2, 50, 10^7)$, dotted line; $(0.2, 250, 10^9)$, solid line; $(0.2, 250, 10^8)$, dashed line; $(0.2, 250, 10^7)$, dashed-dotted line. Bottom: $(\dot{V}, \dot{q}_w, N) = (0.1, 500, 10^9)$, $*$; $(0.1, 500, 10^8)$, $+$; $(0.1, 500, 10^7)$, $\times$; $(0.1, 1500, 10^9)$, $\circ$; $(0.1, 1500, 10^8)$, $\bullet$; $(0.1, 1500, 10^7)$, dotted line; $(0.1, 3000, 10^9)$, solid line; $(0.1, 3000, 10^8)$, dashed line; $(0.1, 3000, 10^7)$: dashed-dotted line).

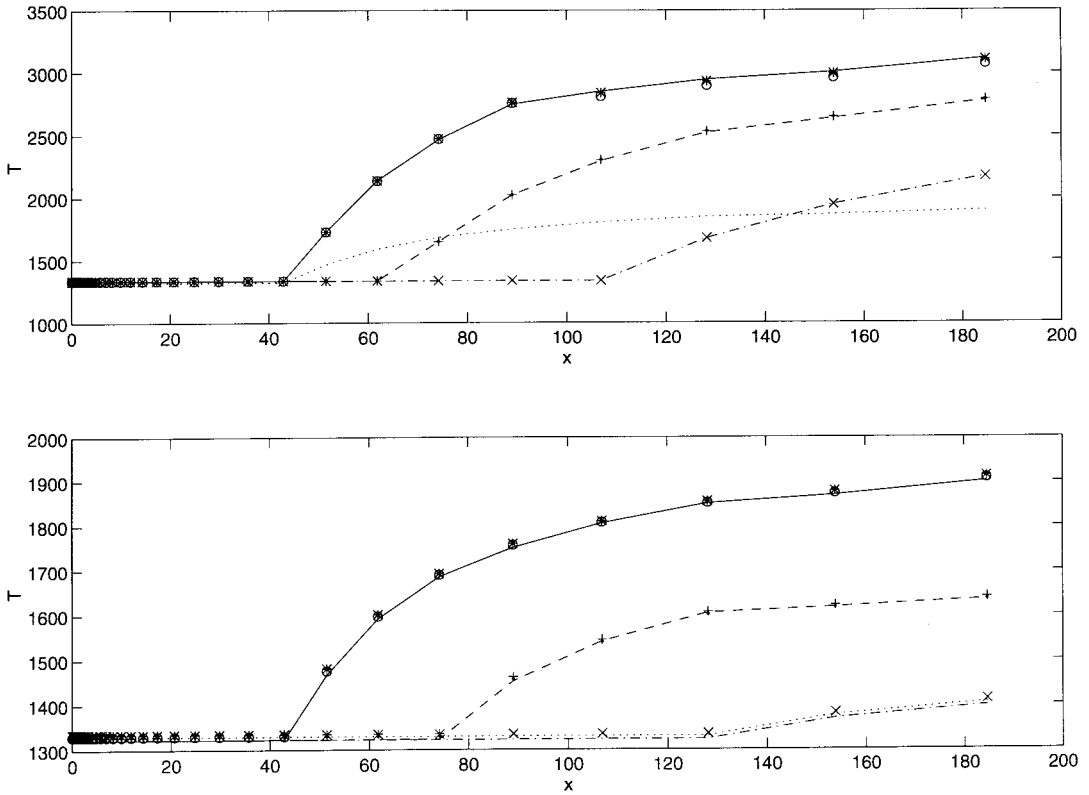

Figure 16. Wall temperature (°C) for fissures along the dyke for the Bingham's model of magmas for an inlet temperature of 1337°C; (Top: $(\dot{V}, \dot{q}_w, N) = (0.2, 50, 10^9)$, $*$; $(0.2, 50, 10^8)$, $+$; $(0.2, 50, 10^7)$, $\times$; $(0.2, 100, 10^9)$, $\circ$; $(0.2, 50, 10^8)$, $\bullet$; $(0.2, 50, 10^7)$, dotted line; $(0.2, 250, 10^9)$, solid line; $(0.2, 250, 10^8)$, dashed line; $(0.2, 250, 10^7)$, dashed-dotted line. Bottom: $(\dot{V}, \dot{q}_w, N) = (0.1, 500, 10^9)$, $*$; $(0.1, 500, 10^8)$, $+$; $(0.1, 500, 10^7)$, $\times$; $(0.1, 1500, 10^9)$, $\circ$; $(0.1, 1500, 10^8)$, $\bullet$; $(0.1, 1500, 10^7)$, dotted line; $(0.1, 3000, 10^9)$, solid line; $(0.1, 3000, 10^8)$, dashed line; $(0.1, 3000, 10^7)$, dashed-dotted line).

of paramount importance to have an adequate rheological model and a good understanding of the heat exchanges with the surrounding rocks.

Finally, it must be noted that the results presented here indicate that, regardless of the magma rheology, the axial velocity component of the magma in the core region can be represented accurately by a parabolic profile, and since the transverse velocity component is much smaller than the axial one while the pressure is almost the hydrostatic one, simpler models of magma ascent in volcanic conduits may be easily derived by using these flow characteristics and accounting in a more detailed manner for the heat transfer from/to the surrounding rocks.

ACKNOWLEDGMENTS

The research reported in this paper was supported in part by Contract No. CEC-EV-5V-CT92-0190 from the Commission of the European Communities. A short version of this paper was presented at the Tenth International Conference on Numerical Methods for Laminar and Turbulent Flow held in Swansea, UK, 21st–25th July, 1997. The author kindly acknowledges Professor Saatdjian's invitation to submit an extended paper for publication in this journal.

REFERENCES

1. J.R. Lister, 'The solidification of buoyancy driven flow in a flexible-walled channel. Part 1. Constant-volume release', *J. Fluid Mech.*, **272**, 21–44 (1994).
2. J.R. Lister, 'The solidification of buoyancy driven flow in a flexible walled channel. Part 2. Continual release', *J. Fluid Mech.*, **272**, 45–65 (1994).
3. P.M. Bruce and H.E. Huppert, 'Thermal control of basaltic fissure eruptions', *Nature*, 16, 665–667 (1989).
4. D.A. Spence and D.L. Turcotte, 'Magma-driven propagation of cracks', *J. Geophys. Res.*, **90**, 575–580 (1985).
5. J.R. Lister and P.L. Dellar, 'Solidification of pressure-driven flow in a finite rigid channel with applications to volcanic eruptions', *J. Fluid Mech.*, **323**, 267–283 (1996).
6. J.J. Wylie and J.R. Lister, 'The effects of temperature-dependent viscosity on flow in a cooled channel with application to basaltic fissure eruptions', *J. Fluid Mech.*, **305**, 239–261 (1995).
7. K.R. Helfrich, 'Thermo-viscous fingering of flow in a thin gap: A model of magma flow in dikes and fissures', *J. Fluid Mech.*, **305**, 219–238 (1995).
8. J.I. Ramos and F. Dobran, 'Magma ascent model development', in: F. Dobran (ed.), *Magma and Lava Flow Modeling and Volcanic System Definition Aimed at Hazard Assessment at Etna*, Giardini, Pisa, Italy, 1994, pp. 71–108.
9. W.D. Bennon and F.P. Incropera, 'Numerical analysis of binary solid–liquid phase change using a continuum model', *Numer. Heat Transf.*, **13**, 277–296 (1988).
10. C.M. Oldenburg and F.J. Spera, 'Hybrid model for solidification and convection', *Numer. Heat Transf. B*, **21**, 217–229 (1992).
11. S.V. Patankar, *Numerical Heat Transfer and Fluid Flow*, Hemisphere, New York, 1980.
12. C. Prakash and V. Voller, 'On the numerical solution of continuum mixture model equations describing binary solid–liquid phase change', *Numer. Heat Transf. B*, **15**, 171–189 (1989).
13. C.R. Carrigan, G. Schubert and J.C. Eichelberger, 'Thermal and dynamical regimes of single- and two-phase magmatic flow in dykes', *J. Geophys. Res.*, **97**, 17377–17392 (1992).
14. H. Pinkerton and R.J. Stevenson, 'Methods of determining the rheological properties of magmas at subliquidus temperatures', *J. Volcanol. Geotherm. Res.*, **53**, 47–66 (1992).
15. I.A. Frigaard, S.D. Howison and I.J. Sobey, 'On the stability of Poiseuille flow of a Bingham fluid', *J. Fluid Mech.*, **263**, 133–150 (1994).

